Identifying explosives by dielectric properties obtained through wide-band millimeter-wave illumination

James C. Weatherall, Jeffrey Barber, Barry T. Smith

James C. Weatherall, Jeffrey Barber, Barry T. Smith, "Identifying explosives by dielectric properties obtained through wide-band millimeter-wave illumination," Proc. SPIE 9462, Passive and Active Millimeter-Wave Imaging XVIII, 94620F (19 May 2015); doi: 10.1117/12.2177216

SPIE.

Event: SPIE Defense + Security, 2015, Baltimore, Maryland, United States

Identifying Explosives by Dielectric Properties Obtained Through Wide-Band Millimeter-Wave Illumination

James C. Weatherall[a], Jeffrey Barber[a], and Barry T. Smith[b]

[a]Battelle Memorial Institute, 2900 Fire Road, Egg Harbor Township, NJ 08234, USA;
[b]U.S. Dept. of Homeland Security, S&T Directorate, Transportation Security Laboratory, W.J. Hughes Technical Center, Atlantic City, NJ 08405

ABSTRACT

A method for extracting dielectric constant from free-space 18 – 40 GHz millimeter-wave reflection data is demonstrated. The reflection coefficient is a function of frequency because of propagation effects, and numerically fitting data to a theoretical model based on geometric optics gives a solution for the complex dielectric constant and target thickness. The discriminative value is illustrated with inert substances and military sheet explosive. In principle, the measurement of reflectivity across multiple frequencies can be incorporated into Advanced Imaging Technology (AIT) systems to automatically identify the composition of anomalies detected on persons at screening checkpoints.

Keywords: Millimeter wave measurement, reflectometry, parameter extraction, dielectric measurement, detection algorithms, explosives detection.

1. INTRODUCTION

Millimeter wave imaging is employed in Advanced Technology Imaging (AIT) systems to screen personnel for concealed explosives and weapons. AIT systems deployed in airports auto-detect potential threats by highlighting the threat location on a generic human shape using imaging data collected over a range of frequency, but lack specificity in threat classification. We demonstrate here a method for extracting dielectric constant from the broad-band free-space reflection data, choosing centimeter and millimeter waves in the frequency range of 18 – 40 GHz. The reflection coefficient is a function of frequency because of propagation effects that relate to the materials complex dielectric constant. By numerically fitting the reflection coefficient as a function of frequency to a theoretical model based on geometric optics, a solution can be found for the complex dielectric constant. Spectral fitting, which has application in optical coherence tomography,[1] enables dielectric detection without a priori knowledge of the material thickness, unlike standard reflection measurement algorithms.[2,3]

The measurement of dielectric constant, including dielectric loss, from the reflection data provides signatures useful for threat identification. In this paper, the method is demonstrated with inert substances and a military sheet explosive to show that detected reflection data can discriminate the materials in a two-dimensional dielectric space. In principle, the detection of reflection coefficient using multiple frequencies can be incorporated into Advanced Imaging Technology (AIT) and standoff imaging systems to provide identifying data on the composition of potential threats, which would allow threat assessment to be accomplished within the scope of millimeter wave screening.

2. EXPERIMENTAL SETUP

Reflection data are collected on samples configured as 15 × 30 cm flat sheets of 1 cm nominal thickness. The samples are backed by a metal plate as a surrogate for a human background, where skin is known to be highly reflective in millimeter waves.[4] S-parameter S_{11} data is collected in polar form using an Agilent N5245A PNA-X network analyzer and a Q-par WBH18-40 wide band horn. The horn is positioned at a distance of 34.5 cm from the samples, which is outside the Fraunhofer distance, but close enough to keep the main beam within the sample to circumvent edge diffraction effects.

Passive and Active Millimeter-Wave Imaging XVIII, edited by David A. Wikner, Arttu R. Luukanen, Proc. of SPIE Vol. 9462, 94620F · © 2015 SPIE
CCC code: 0277-786X/15/$18 · doi: 10.1117/12.2177216

The measurements are calibrated to a reference plane at the backing surface, using a one-port error model determined with S_{11} measurement from the backing metal plate, a metal plate offset a short distance relative to wavelength, and an absorber.[5,6] The purpose of the calibration is to relate the S-parameter measurement to the fields at the surface of the sample. For example, in terms of the field E_0 outgoing from the antenna, and the field E_1 returning, the reflection S-parameter is defined $S_{11} = E_1 \,/\, E_0$. However, the reflection coefficient is defined at the surface of the sample, where the incoming and outgoing radiation fields are E_{in} and E_{out}, and the reflection coefficient is given by $r = E_{out} \,/\, E_{in}$. In terms of measured S_{11} parameter, the reflection coefficient is computed through the reduced calibration coefficients a, b, and c, which are solved from the S-parameters collected from the three calibration data sets:

$$r = \frac{S_{11} - b}{a - cS_{11}} \ . \tag{1}$$

The calibration compensates not only for propagation through space, but for errors due spurious reflections in cabling and multiple paths to the antenna.

The effect of the calibration is demonstrated in Figure 1, which shows the S-parameter measurement and calibrated reflection coefficient data from a reflecting plate. Three calibrations were averaged, with offsets of 0.102, 0.204, and 0.306 cm. Figure 1(a) shows the S-parameter data measured for a metal plate at a distance 0.408 cm from the reference plane 34.5 cm distant from the horn with no correction applied. Figure 1(b) shows the calibrated reflection coefficient. The calibration produces a mean reflection coefficient of magnitude 1.03 for a metallic plate across the band 18 - 40 GHz, with standard deviation of ±0.04.

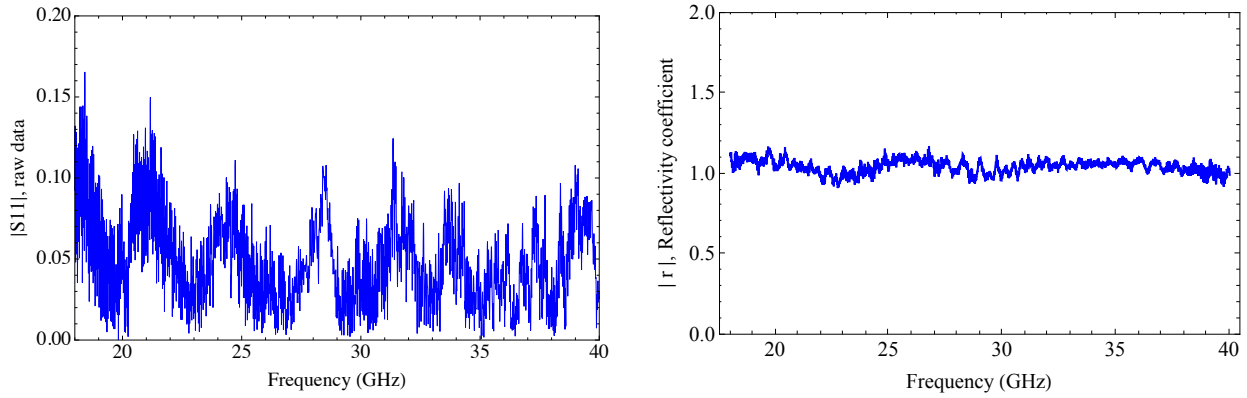

(a) (b)

Figure 1: Reflection magnitude of offset plate: (a) direct S-parameter measurement; (b) calibrated reflection coefficient.

3. DATA

Data are collected on three materials with thicknesses ranging 1 – 1.25 cm, and backed with a metal plate: 1) transparent plastic (Lexan); 2) paper (20 lb. sheet); and 3) a PETN-based rubberized sheet explosive, Primasheet 1000 (P1000). The basic phenomenology is illustrated in the time domain, which can be constructed from the calibrated reflection spectrum by Fourier transform (see Figure 2). The time origin is set as zero from the calibration plane. The first return (negative time displacement) is the partial reflection from the front surface, and the second return is from the reflection on the backing layer after twice traversing the sample. Energy absorbed in the material diminishes the second reflection.

The time domain data illustrate some of the elements of imaging signatures; foremost of these are time-resolved reflections, and their time separations and magnitude. Although the front surface reflection is a small part of the total return, it is intrinsic to the index of refraction. The intensities of the second reflection vary

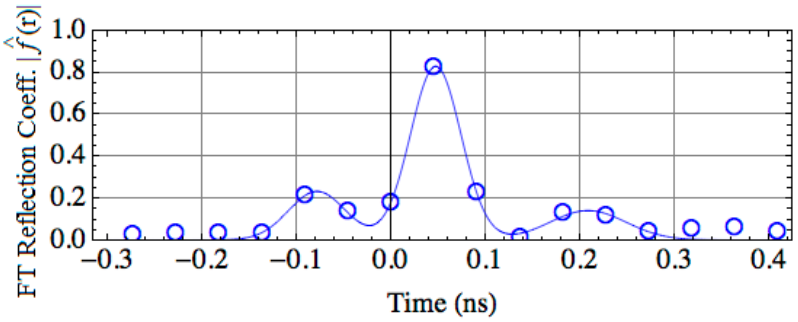

(a)

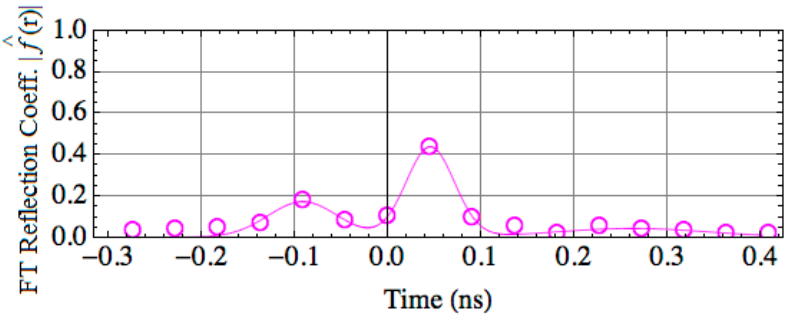

(b)

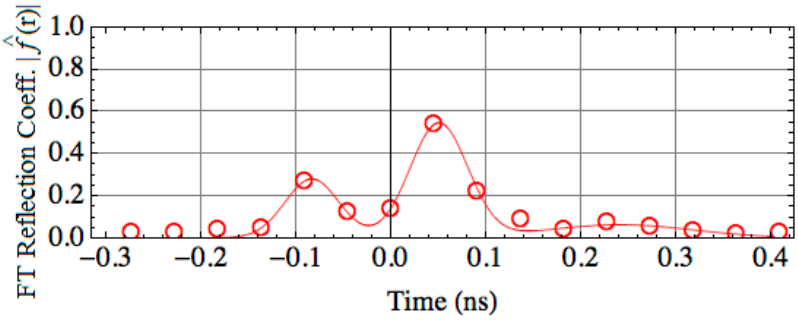

(c)

Figure 2: Time domain of pulsed reflection amplitude: (a) Lexan; (b) Paper; (c) P1000. Lines are fits to data

according to absorption in the material – the loss in the Lexan being smaller than the other materials. The time series imparts information on refractive index, particularly as it affects front surface reflection coefficient, time delay, total reflection coefficient, and phase.[7–9] The challenge to analyzing the time series is that the reflection exhibits only a handful of points, and poorly resolves the location of the peaks. The time resolution in the time domain is $1 / \Delta \sim 0.045$ ns, where Δ is the frequency bandwidth, and so the resolution is on the same order as the measured time delays.

Generally, images constructed from the time domain data have little discriminative value unless the surface reflections are well resolved and separated in time. The greater potential for discriminating among materials with similar reflection coefficient is realized when the data are parsed in frequency, i.e., as a reflection spectrum. The frequency reflection spectra for our three materials are shown in Figure 3. The oscillations are due to constructive and destructive interference among multiple reflections. Manifest differences can be observed in frequency spacing between interference maxima, the amplitude range between maximum and minimum, and change in reflection coefficient across frequency. In Section 4, we show how these spectral attributes relate to the physical properties and configuration of the material, and can be exploited for material identification.

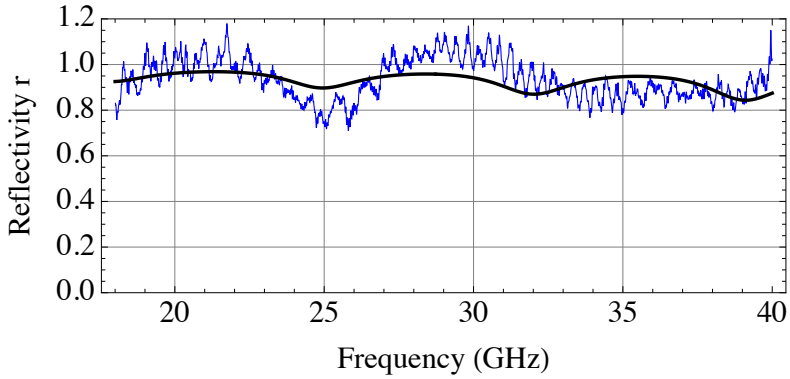

(a)

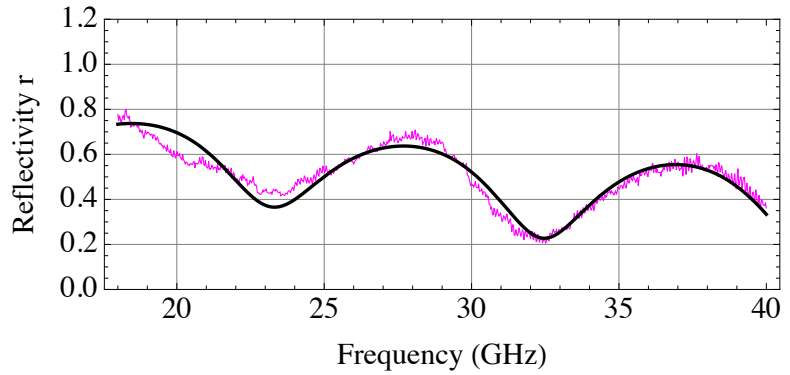

(b)

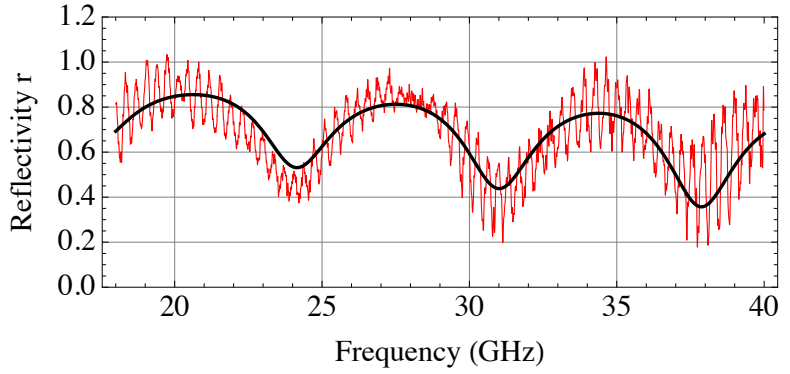

(c)

Figure 3: Frequency spectra of reflection coefficient magnitude: (a) Lexan; (b) Paper; (c) P1000. Lines are models described in Section 5.

4. THEORY

The intensity of millimeter radiation observed from illumination of a target material depends on the values of the real and imaginary components of the complex dielectric constant, and its geometric thickness. These three parameters determine the total of the radiation returned from the material through reflection from the outer surface, and transmission and reflection from the internal interface of the material with the body, and are quantified with an optical model.

The reflection coefficient model is a straightforward application of Fresnel's equations for optical reflection and transmission through interfaces of materials with different refractive index.[10,11] We consider a system with two interfaces with three components: the backing material, "2", the sample material, "1", and air, "0", are indicated schematically in Figure 4. The indices of refraction are denoted as n_2, n_1, and n_0, respectively. In general, the index is a complex quantity. Reflection and transmission coefficients are ratios of the respective electric fields relative to the incident electric field, inclusive of phasing.

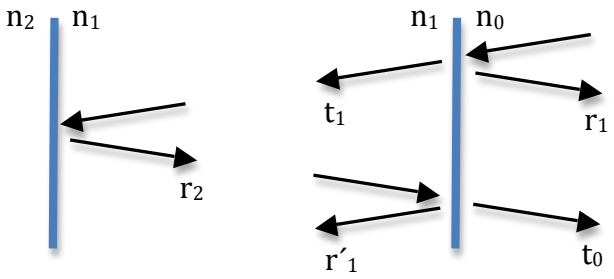

Figure 4: Reflection and transmission at the interfaces of layered materials of three different refractive indices.

The reflection and transmission coefficients for fields propagating from 0 to 1 (in normal incidence) are

$$r_1 = \frac{n_1 - n_0}{n_1 + n_0} \; ; \tag{2}$$

$$t_1 = \frac{2n_1}{n_1 + n_0} \; . \tag{3}$$

The reflection coefficient at the interface 1 to 2 is

$$r_2 = \frac{n_2 - n_1}{n_2 - n_1} \; . \tag{4}$$

And, the reflection and transmission coefficients for fields propagating outward from 1 to 0 are

$$r_1' = \frac{n_0 - n_1}{n_0 + n_1} \; ; \tag{5}$$

$$t_0 = \frac{2n_0}{n_1 + n_0} \; . \tag{6}$$

The total of the reflected electric field has contributions from reflections on the front and back surface, and multiple internal reflections escaping the slab. The sum of the fields, normalized to the incident field to give the reflection coefficient, is written

$$r = r_1 e^{i\theta_0} + t_0 r_2 t_1 (e^{i\theta_1} + (r_1' r_2) e^{i\theta_2} + (r_1' r_2)^2 e^{i\theta_3} + \cdots) \; , \tag{7}$$

where θ_m represents the phase incremented by the propagation. The phasing constant for m-propagations to-and-from the front and back surface separated by a thickness ΔL is

$$\theta_m = \theta_0 + m\, n_1 (2f/c)\; (2\Delta L) \; . \tag{8}$$

The imaginary component of n_1 in the phase term accounts for absorption. Eq. 7 can be simplified by summation formula for an infinite geometric series.[10–12] For our purpose, the sum can usually be truncated at five or fewer terms. Leaving the reflection coefficient in the form of Eq. 7 allows modification to incorporate phase error,

such as due to surface irregularity. The overall phase is a function of the displacement of the front surface, $\theta_0 = -(2f/c)(2\Delta L)$.

In terms of this model, the properties of an unknown slab of material on a backing substance of known dielectric – in this case, metal – is characterized by three parameters: the thickness, ΔL; and n_1' and n_1'', which are the real and imaginary components of the refractive index, $n_1 = n_1' + in_1''$.

In principle, these parameters can be deduced from a minimum of three observational aspects:

1. Examination of Eq. 8 shows that absorption varies in proportion to the frequency. Over a range of frequency, the material will vary from transparent to opaque. The total reflection at frequencies where the material is transparent includes reflections from the back surface, whereas at frequencies where the slab is absorbing, the total reflection is from the front surface only. The characteristic frequency where half of the incident radiative energy is lost between front and back surface is
$$f_\tau = \frac{c}{4\pi(\Delta L)n_1''} \ ; \tag{9}$$

2. Constructive and destructive interference is also demonstrated in Eq. 8. For example, the primary reflections from the front and back surface add constructively if $\theta_2 - \theta_1$ is an even integer times π, and destructively if an odd number of π: consecutive maxima will occur at frequency intervals given (approximately) by
$$f_{m+1} - f_m = \frac{c}{2(\Delta L)n_1'} \ ; \tag{10}$$

3. Finally, the asymptotic reflection coefficient is related to the front surface alone, and is independent of thickness:
$$r_\infty = \left| \frac{n_0 - n_1}{n_0 + n_1} \right| \ . \tag{11}$$

In practice, the frequency bandwidth will not be adequate to identify all these attributes of the reflection spectrum. Rather, a least-squares method is used to find a best-fit model to wide-bandwidth data.

5. ANALYSIS

In our analysis, we use the function *NonlinearModelFit* in the MATHEMATICA computing software[13] to match the reflection coefficient model parameters ΔL, n_1', and n_1'' to the experimental data. The fitting is done on the real part of the complex reflection coefficient, r. While the fitting can be done with the amplitude of the reflection coefficient, with similar result, the real (or imaginary) component contains additional information on thickness from phase data. The reflection models for each material are shown overlaid on the complex reflection coefficient in Figure 5.

The parameter solutions are given in Table 1. Sources of error in the solutions include the precision in the numerical model fitting, errors in reflection amplitude (such as calibration and optical errors), and reflection phase (calibration error and deviations from surface flatness). Model fitting error is estimated from confidence intervals from the fitting algorithm. The amplitude error is on the order of 4%, as inferred from the deviation from unity for a metal plate (c.f., Figure 1), and the phase error is estimated at 5 – 20 degrees from the noise in the data. The propagation of these errors into the fitting parameters is exhibited by the error in the last digits given in parenthesis in Table 1. The final two columns give corresponding dielectric constants, which are alternative to characterizing the materials' electromagnetic properties.[14,15] For nonmagnetic materials, the dielectric is computed from the refractive index by $\epsilon = \sqrt{n}$.

Practical application requires that the detected materials must have distinguishable dielectric constants. Figure 6 plots the materials in dielectric space, and shows that the materials are separated from one another. Thus, the method provides a way to detect intrinsic material dielectric properties of reflection anomalies. The dielectric properties of the target may then be compared to a library of dielectric constants to identify the likely composition of the material.

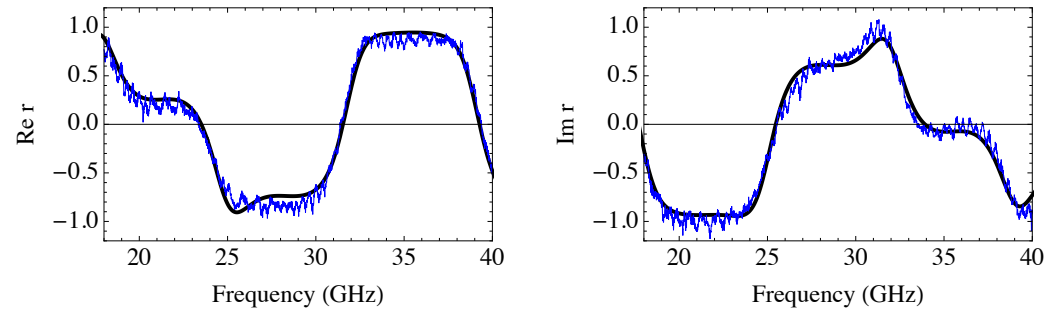

(a)

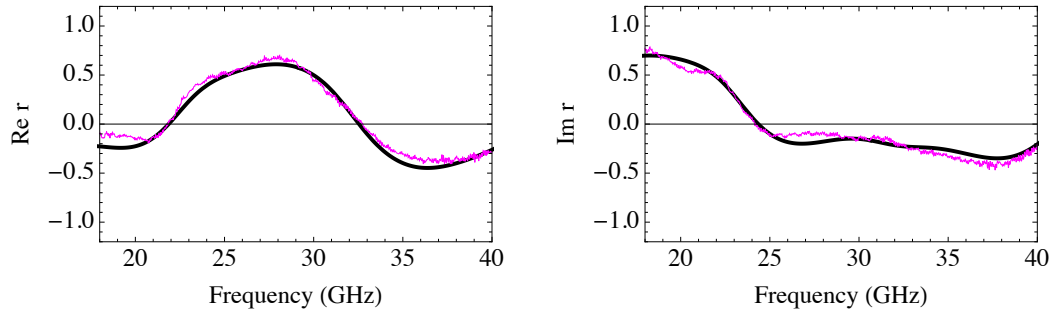

(b)

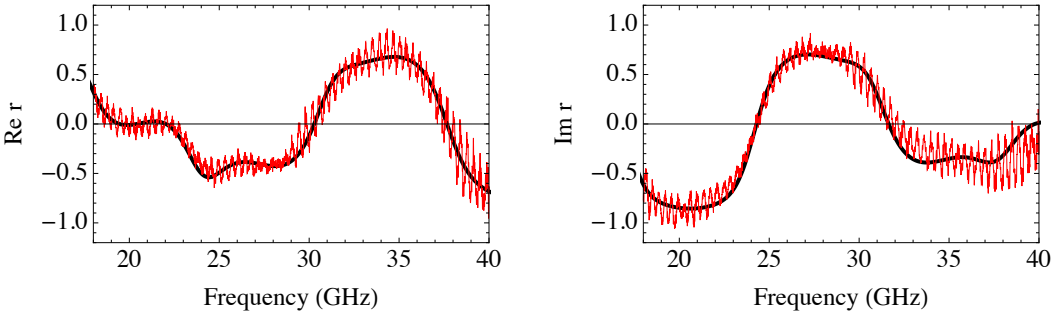

(c)

Figure 5: Model fits to the real part of reflection coefficient are plotted as thick lines on real and imaginary components of the reflection data: top to bottom,: (a) Lexan; (b) Paper; (c) P1000. See Figure 3 for how model fit appears in amplitude.

Table 1: Parameter Solutions and Errors

Material	ΔL_r	n_1'	n_1''	ϵ'	ϵ''
Lexan	1.26(4)	1.68(2)	0.006(06)	2.81(6)	0.02(2)
Paper	1.06(1)	1.53(1)	0.059(11)	2.34(3)	0.18(4)
P1000	1.29(2)	1.69(2)	0.031(07)	2.86(7)	0.11(2)

The ability to discriminate materials will depend on the density of materials in the detection space and measurement precision. The effect of reflection measurements on non-ideal backing materials is as yet unknown, but this should be a matter of extending the model to include a complex refractive index, n_2, for the backing layer, or including additional layers, as necessary.

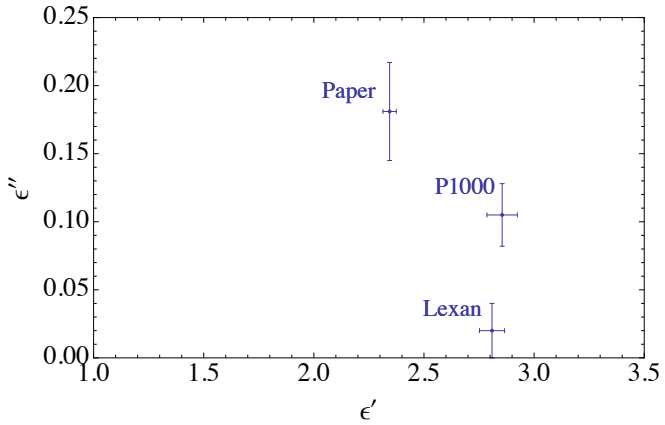

Figure 6: Detected materials in dielectric space.

6. CONCLUSION

The results of this analysis show that the dielectric constant can be detected at modest range to an accuracy on the order of $\pm$ 0.05 in both ϵ' and ϵ'' by fitting the reflection coefficient spectrum across a broad range of frequencies to a suitable optical model. The detection is independent of thickness. In principle, multi-frequency interrogation is established as a way to identify concealed materials on personnel at a checkpoint. The method has the potential to determine whether the detected dielectric matches the dielectric of an identified threat (for example, in a detection library). Alternatively, the detected dielectric might be excluded as a potential threat if it is outside the region of dielectric space occupied by any explosive or non-explosive threat, independently from identification. The converse may also usefully apply, if the detected dielectric is found to be consistent with the parameters of a known benign material associated with the image anomaly.

The frequency band 18 – 40 GHz is only slightly broader than fielded millimeter wave imaging systems, and could potentially be incorporated into current or future imaging systems. Imaging systems that use temporal ranging to interpret the image already collect the conjugate frequency data, albeit over a lesser bandwidth.

Our data were collected in optimal circumstances with the object on a totally reflecting background. Also, only a few representative materials are presented. Additional research is planned to increase the functionality of the techniques, including an imperfectly reflecting background incorporating a surface with dielectric properties similar to skin (i.e., a skin simulant[16]).

ACKNOWLEDGMENTS

Work was performed under DHS Contract HSHQDC-13-A-00023, Transportation Security Laboratory (TSL) Technical Services for Research, Development and Engineering (RD&E); Development Test and Evaluation (DT&E) Task Order No. HSHQDC-13-J-00209 Multi-frequency MMW IDX.

REFERENCES

[1] Tomlins, P. H. and Wang, R. K., "Simultaneous analysis of refractive index and physical thickness by Fourier domain optical coherence tomography," *IEE Proc.-Optoelectron.* **153**, 222–228 (2006).

[2] Fenner, R. A., Rothwell, E. J., and Frasch, L. L., "A comprehensive analysis of free-space and guided-wave techniques for extracting the permeability and permittivity of materials using reflection-only measurements," *Radio Sci.* **47**, RS1004:1–13 (2012).

[3] Weir, W. B., "Automatic measurement of complex dielectric constant and permeability at microwave frequencies," *Proc. IEEE* **62**, 33–36 (1974).

[4] Alekseev, S. I. and Ziskin, M. C., "Human skin permittivity determined by millimeter wave reflection measurements," *Bioelectromagnetics* **28**, 331–339 (2007).

[5] Umari, M. H., Ghodgaonkar, D. K., Varadan, V. V., and Varadan, V. K., "A free-space bistatic calibration technique for the measurement of parallel and perpendicular reflection coefficients of planar samples," *Instrumentation and Measurement, IEEE Transactions on* **40**(1), 19–24 (1991).

[6] Zhao, M., Shea, J. D., Hagness, S. C., and Van Der Weide, D. W., "Calibrated free-space microwave measurements with an ultrawideband reflectometer-antenna system," *Microwave and Wireless Components Letters, IEEE* **16**(12), 675–677 (2006).

[7] Ahmed, S., Ostwald, O., and Schmidt, L., "Automatic detection of concealed dielectric objects for personnel imaging," in [*IEEE MTT-S International Microwave Workshop on Wireless Sensing, Local Positioning, and RFID (IMWS 2009)*], 1–4 (Sept. 2009).

[8] Luukanen, A., Ala-Laurinaho, J., Häkli, J., Gomes-Martins, D., Kiuru, T., Leivo, M., Rautiainen, A., Säily, J., Tamminen, A., Toivanen, H., Tuovinen, R., and Räisänen, A., "Multi-band imaging and adaptive beam-steering techniques for the submillimetre-wave range," in [*7th European Conference on Antennas and Propagation (EuCAP)*], 1946–1948 (Aug. 2013).

[9] Jaruwatanadilok, S., Kuga, Y., and Ishimaru, A., "An electromagnetic model for plastic composite materials under obscuring layers," in [*IEEE International Symposium on Antennas and Propagation (ISAP)*], 4841–4844 (Nov. 2006).

[10] Bohren, C. F. and Huffman, D. R., [*Absorption and Scattering of Light by Small Particles*], Wiley-VCH, Weinheim (2004).

[11] Jackson, J. D., [*Classical Electrodynamics*], Wiley, New York (1999).

[12] Alabaster, C., "Permittivity measurements on human skin in the millimetre wave band," in [*18th International Conference on Applied Electromagnetics and Communications (ICECom 2005)*], 1–4 (Oct. 2005).

[13] Wolfram Research, Inc., [*Mathematica Edition: Version 9.0*], Wolfram Research, Champaign, Illinois (2012).

[14] A. von Hippel, [*Dielectric Materials and Applications*], Artech, Norwood, MA (1995).

[15] Baker-Jarvis, J., Janezic, M. D., Riddle, B., Holloway, C. L., Paulter, N. G., and Blendell, J. E., "Dielectric and conductor-loss characterization and measurements on electronic packaging materials,," *NIST Technical Note* **1520** (2001).

[16] Barber, J., Weatherall, J. C., Greca, J., and Smith, B., "Toward the development of an image quality tool for the testing of active millimeter wave imaging systems," in [*SPIE 2015, this conference*], (Apr. 2015).